Ruthenium(VI) Doped into Single Crystals with the $BaSO_4$ and β-K_2SO_4 Structures: Optical Absorption Spectra of RuO_4^{2-}

Thomas C. Brunold and Hans U. Güdel*

Departement für Chemie, Freiestrasse 3, Universität Bern, CH-3000 Bern 9, Switzerland

Received October 31, 1996[⊗]

By establishing suitable high-temperature preparation conditions we were able to grow the first RuO_4^{2-}-doped crystals of K_2CrO_4, K_2SeO_4, Cs_2MoO_4, $BaSO_4$, $BaCrO_4$, and $BaSeO_4$. Their polarized absorption spectra at low temperatures are reported and discussed. These are very different from the ruthenate(VI) spectra in the literature, and the lack of resemblance between calculated and measured spectra of ruthenate(VI)—assumed to be RuO_4^{2-} in the past—is easily understood. The $^3A_2 \rightarrow {}^1A_1$ spin-flip transition of RuO_4^{2-} peaks at ≈7100 cm^{-1}. Stronger bands due to $^3A_2 \rightarrow {}^3T_2$ and $^3T_1$ are observed in the vis around 13 500 and 16 500 cm^{-1}, respectively, giving rise to the green-blue color of most samples. In the $BaSO_4$ host the $^1A_1$ absorption line is split into three differently polarized components exhibiting a strong temperature dependence. This can be analyzed in terms of a Boltzmann population with three levels at 0, 13, and 18 cm^{-1}, corresponding to the three spinor components of the $^3A_2$ ground state. In order to better understand the major changes which occur on going from the $3d^2$ to the $4d^2$ electron configuration the spectroscopic data of RuO_4^{2-} are compared with those of CrO_4^{4-}, MnO_4^{3-}, and FeO_4^{2-}.

1. Introduction

Basic aqueous solutions of oxygenated ruthenium(VI)—known as ruthenate(VI) ion—are of considerable importance in both analytical and synthetic chemistry, and the rather puzzling absorption spectrum has attracted much interest for many years. For the spectrophotometric determination of ruthenium the compounds are fused with a mixture of potassium hydroxide and potassium nitrate, and the resulting cake is dissolved in water.[1−4] In every case a clear orange-red solution of ruthenate(VI) with maximum absorbance at 465 nm (21 500 cm^{-1}) is obtained. The solid line in Figure 1 shows the well-known absorption spectrum of a ruthenate(VI) solution 10 M in KOH.

Many ruthenium(VI) complexes are effective catalysts for the selective oxidation of various organic substrates either in their own right or in conjunction with other species. Basic aqueous solutions of ruthenate(VI) with persulfate as co-oxidant are used to oxidize primary and secondary alcohols to carboxylic acids and ketones, respectively, aldehydes to carboxylic acids, and activated primary and secondary alkyl halides to carboxylic acids and ketones, respectively.[5−7] The ruthenate/$S_2O_8^{2-}$ reagent is both aesthetically and practically attractive in that it is self-indicating, the orange color becoming black on addition of substrate and returning to its original color when the oxidation reaction is complete. These color changes have been explained in terms of an initial reduction of ruthenate(VI) to RuO_2 and a subsequent reoxidation by $S_2O_8^{2-}$.[7]

In analogy to the $3d^2$ tetroxo complexes CrO_4^{4-}, MnO_4^{3-}, and FeO_4^{2-}, the ruthenate(VI) ion with the $4d^2$ electron configuration was thought to be RuO_4^{2-} until about 20 years ago. Accordingly, similar approaches were used for the interpretation of the absorption spectra of the $3d^2$ tetraoxo complexes and the ruthenate(VI) ion.[8−12] While the calculations were quite successful in the description of the energy-level structures of the $3d^2$ systems, the assignment of the ruthenate(VI) spectrum has remained unclear. In particular, the weak $d \rightarrow d$ bands peaking around 12 000 cm^{-1} in the spectra of the $3d^2$ complexes have not yet been observed for ruthenate(VI) (see Figure 1).

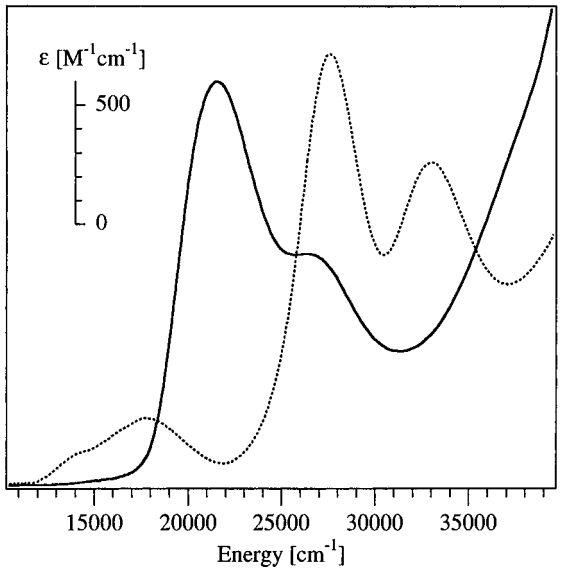

Figure 1. Unpolarized room-temperature absorption spectra of a ruthenate(VI) solution 10 M in KOH (solid line) and RuO_4^{2-} doped into $BaSO_4$ (dotted line).

In 1976 the structure of so-called barium ruthenate monohydrate, $BaRuO_4 \cdot H_2O$, was determined[13] and ruthenium(VI) was

[⊗] Abstract published in *Advance ACS Abstracts,* April 1, 1997.

(1) Richard, R. R.; Marshall, E. D. *Anal. Chem.* **1950**, *22*, 795.
(2) Connick, R. E.; Hurley, C. R. *J. Am. Chem. Soc.* **1952**, *74*, 5012.
(3) Stoner, G. A. *Anal. Chem.* **1955**, *27*, 1186.
(4) Woodhead, J. L.; Fletcher, J. M. *J. Chem. Soc.* **1961**, 5039.
(5) Schröder, M.; Griffith, W. P. *J. Chem. Soc., Chem. Commun.* **1979**, 58.
(6) Green, G.; Griffith, W. P.; Hollinshead, D. M.; Ley, S. V.; Schröder, M. *J. Chem. Soc., Perkin Trans.* 1 **1984**, 681.
(7) Bailey, A. J.; Griffith, W. P.; Mostafa, S. I.; Sherwood, P. A. *Inorg. Chem.* **1993**, *32*, 268.
(8) Carrington, A.; Jørgensen, C. K. *Mol. Phys.* **1961**, *4*, 395.
(9) Viste, A.; Gray, H. B. *Inorg. Chem.* **1964**, *3*, 1113.
(10) Gray, H. B. *Coord. Chem. Rev.* **1966**, *1*, 2.
(11) Rauk, A.; Ziegler, T.; Ellis, D. E. *Theor. Chim. Acta* **1974**, *34*, 49.
(12) Ziegler, T.; Rauk, A.; Baerends, E. J. *Chem. Phys.* **1976**, *16*, 209.
(13) Nowogrocki, P. G.; Abraham, F.; Tréhoux, J.; Thomas, D. *Acta Crystallogr., Sect. B: Struct. Crystallogr. Cryst. Chem.* **1976**, *B32*, 2413.

S0020-1669(96)01314-6 CCC: $14.00

found in a trigonal-bipyramidal configuration consisting of three oxygens and two hydroxides, i.e. *trans*-$Ru(OH)_2O_3^{2-}$. Subsequently it turned out that in potassium ruthenate, nominally known as $K_2RuO_4 \cdot H_2O$, the Ru(VI) ion has an analogous trigonal-bipyramidal configuration and that the appropriate formula is thus $K_2Ru(OH)_2O_3$.[14,15] Both the barium and potassium compounds are deep red in color. In contrast, in Cs_2RuO_4 prepared by a solid-state reaction at 800 °C, the Ru(VI) ion was quite recently found to be tetrahedrally coordinated by four oxygens.[16] Interestingly, these crystals are dark green rather than red in color. It appears obvious, therefore, that the species which causes the orange-red color of the ruthenate(VI) solution is actually *trans*-$Ru(OH)_2O_3^{2-}$.

In the present study we report the preparation and optical spectroscopy of the first RuO_4^{2-}-doped single crystals. The aim of this contribution is to elucidate the energy-level scheme for RuO_4^{2-}, a problem which has not been solved yet due to lack of experimental data. The absorption spectrum of the $4d^2$ ion RuO_4^{2-} is, as expected, similar to the spectra of tetrahedrally oxo-coordinated $3d^2$ ions. In contrast, as we demonstrate in Figure 1, it differs substantially from the ruthenate(VI) solution spectrum. The failure to reproduce the measured spectrum of ruthenate(VI)—assumed to be RuO_4^{2-} in the past—is readily understood. In the $BaSO_4$ host the low-temperature absorption spectra are strongly polarized, thus allowing a detailed study of the energy-level structure of RuO_4^{2-}. Finally, the spectroscopic data of RuO_4^{2-} are compared with those of the series of $3d^2$ ions CrO_4^{4-}, MnO_4^{3-}, and FeO_4^{2-}.

2. Experimental Section

2.1. Sample Preparation. We have prepared RuO_4^{2-}-doped single crystals of K_2CrO_4, K_2SeO_4, and Cs_2MoO_4 with the β-K_2SO_4 structure and $BaSO_4$, $BaCrO_4$, and $BaSeO_4$ with the barite structure. Both structures crystallize in the orthorhombic space group *Pnma*.[17] In these structures there are four crystallographically equivalent MO_4^{2-} ions (M is either S, Cr, Se, or Mo) per unit cell with a mirror plane perpendicular to the crystallographic **b** axis as the only symmetry element.

β-K_2SO_4 type hosts are soluble in water, and single crystals doped with the $3d^2$ ion FeO_4^{2-} are easily obtained by slowly evaporating basic aqueous hypochlorite (ClO^-) solutions saturated with the appropriate host.[18] However, attempts to grow RuO_4^{2-}-doped crystals using similar methods were unsuccessful, presumably due to the five-coordinate configuration of Ru(VI) in aqueous solution. In order to obtain RuO_4^{2-}-doped samples we thus had to resort to other techniques.

Single crystals of RuO_4^{2-}-doped K_2CrO_4 and K_2SeO_4 were grown by the flux-evaporation method using a mixture of KNO_3 and KOH as flux medium. Best results were obtained with the weight compositions KNO_3 (40%), KOH (40%), K_2CrO_4 (20%), or K_2SeO_4 (20%). $K_2Ru(OH)_2O_3$ was added in concentrations of 2 mol % with respect to the hosts, and the mixtures were homogenized and fired in air for 10 h at 450 °C and another 65 h at 440 °C using corundum boats. The green crystals of K_2CrO_4:Ru^{6+} obtained by this method have dimensions up to $2 \times 1 \times 1$ mm^3. The K_2SeO_4:Ru^{6+} crystals are slightly smaller and turquoise in color. Black residues in the corundum boats indicated the partial formation of RuO_2 during crystal growth, and the actual Ru concentration in the samples is thus lower than 2 mol %.

Cs_2MoO_4 crystals nominally doped with 0.5 mol % RuO_4^{2-} were prepared by the solid-state reaction of Cs_2CO_3, MoO_3, and $K_2Ru(OH)_2O_3$ in the appropriate molar amounts at 950 °C in a platinum crucible in air. Small crystals could be separated from the polycrystalline melt. Their color is green but gradually changes to orange in air. These crystals are hygroscopic, and the color change indicates the transition of RuO_4^{2-} to the *trans*-$Ru(OH)_2O_3^{2-}$ complex.

Barite-type mixed single crystals of $BaMO_4$:Ru^{6+} (M = S, Cr, or Se) were grown from a NaCl−KCl flux using the weight compositions NaCl (32%), KCl (43%), and $BaMO_4$ (25%). $K_2Ru(OH)_2O_3$ was added in concentrations of 0.1 and 1 mol % with respect to $BaMO_4$ for absorption measurements in the UV/vis and near-infrared (near-IR) regions, respectively. The starting materials were thoroughly mixed, fired for 12 h at 750 °C in air, and slowly cooled to 650 °C at −2.5 °C/h using platinum crucibles with tight-fitting lids. In the case of the 0.1 mol % doped samples of $BaSO_4$ we found no signs of RuO_2 formation and thus used the nominal Ru concentration to calculate extinction coefficients and oscillator strengths. The size of the crystals approaches $4 \times 1.5 \times 2$ mm^3 along the **a**, **b**, and **c** axes, respectively. The axes are readily identified from the crystal morphology. The color of Ru(VI) doped samples of $BaSO_4$ and $BaSeO_4$ is blue-gray and that of $BaCrO_4$:Ru^{6+} is brown due to the yellow color of the host. Crystals of $BaSO_4$:Ru^{6+} are strongly dichroic. They are deep blue, green, and red in color for linearly polarized light with **E** parallel to **a**, **b**, and **c**, respectively.

For the assignment of an absorption line in the infrared (see section 4.1) we prepared a $BaSO_4$:Ru^{6+} sample under different conditions. Using the weight composition NaCl (13%), KCl (18%), CsCl (64%), and $BaSO_4$ (5%), we were able to grow $BaSO_4$:Ru^{6+} crystals between 620 and 450 °C. These crystals are slightly worse in optical quality compared to those grown from a NaCl−KCl flux, and interestingly, they grew elongated along **b** rather than **a**.

2.2. Absorption Measurements. Absorption spectra were recorded on a double-beam spectrometer (Cary 5e) and, in the region below 4000 cm^{-1} (>2.5 μm), a Fourier transform infrared spectrometer (Perkin-Elmer 1720 X) purged with N_2. For sample cooling to 15 K a closed-cycle helium refrigerator (Air Products) was used, and variable temperatures between 6 and 100 K were achieved with a cold helium-gas flow technique.

In the β-K_2SO_4 structure Ru(VI) occupies a site for which the **E**||**a** and **E**||**c** spectra are essentially identical. Polarized absorption spectra of RuO_4^{2-} in that structure were thus recorded with **E** parallel and perpendicular to the **b** axis.

Absorption spectra of $BaMO_4$:Ru^{6+} (M = S, Cr, Se) were measured with **E** parallel to the crystallographic **a**/**b** and **b**/**c** axes of crystals polished perpendicular to **c** and **a**, respectively. We will show in section 4.2 that crystals with the barite structure are very favorable hosts for RuO_4^{2-} in that the polarized crystal spectra correspond, in essence, to the polarized molecular spectra. The strong molecular polarizations thus give rise to the strongly polarized crystal spectra presented in the following.

3. Results

The polarized 15 K absorption spectra of $BaSO_4$:Ru^{6+} for **E** parallel to **a**, **b**, and **c** are shown in Figure 2. In the near-infrared (near-IR) region a very weak sharp line peaks at about 7320 cm^{-1} (labeled $^1A_1$ in Figure 2). The spectral region between 11 000 and 23 000 cm^{-1} consists of a highly polarization-dependent band system. In each polarization we observe a poorly structured broad band (denoted by $^3T_1$) with a shoulder ($^3T_2$) on its low-energy side. Above 23 000 cm^{-1} two very intense bands are observed in all three polarizations. They are very similar in position to the two lowest-energy bands observed in the spectra of RuO_4 and RuO_4^-,[2] and it is thus relatively straightforward to assign them to O → Ru ligand-to-metal charge-transfer (LMCT) transitions. Note that in **b** polarization the LMCT 1 band has a distinct shoulder around 23 500 cm^{-1}.

The **E**||**a**, **E**||**b**, and **E**||**c** polarized 15 K absorption spectra of $BaSO_4$:Ru^{6+} in the 10 000−23 500 cm^{-1} region are reproduced in Figure 3 as solid lines. In these graphs the dotted curves were obtained from fits of two Gaussians to the experimental spectra, and the broken lines show the sums of each pair of fitted curves. Comparison of the measured and calculated spectra shows that the correspondence is very good. The fitted parameters together with the oscillator strengths *f*

(14) Elout, M. O.; Haije, W. G.; Maaskant, W. J. A. *Inorg. Chem.* **1988**, *27*, 610.
(15) Fischer, D.; Hoppe, R. *Z. Anorg. Allg. Chem.* **1991**, *601*, 41.
(16) Fischer, D.; Hoppe, R. *Z. Anorg. Allg. Chem.* **1990**, *591*, 87.
(17) (a) Wyckoff, R. W. G. *Crystal Structures*, 2nd ed.; Interscience: New York, 1965; Vol. 3; pp 45−47. (b) McGinnety, J. A. *Acta Crystallogr. B* **1972**, *28*, 2845. (c) Gattow, G. *Acta Crystallogr.* **1962**, *15*, 419. (d) Gonschorek, W.; Hahn, Th. *Z. Kristallogr.* **1973**, *138*, 167.
(18) Brunold, T. C.; Hauser, A.; Güdel, H. U. *J. Lumin.* **1994**, *59*, 321.

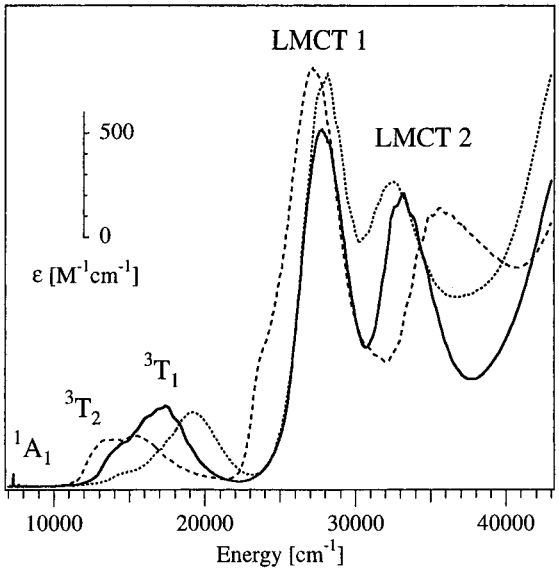

Figure 2. **E**||**a** (solid line), **E**||**b** (broken line), and **E**||**c** (dotted line) polarized absorption spectra of $BaSO_4$:Ru^{6+} at 15 K. $d \rightarrow d$ band designations are given in the T_d parent symmetry. O $\rightarrow$ Ru ligand-to-metal charge-transfer bands are labeled LMCT 1/2.

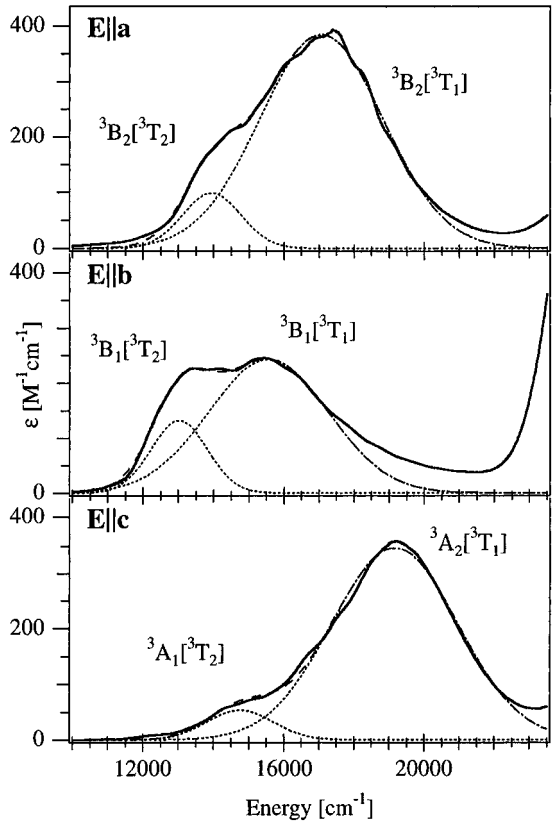

Figure 3. **E**||**a**, **E**||**b**, and **E**||**c** polarized $d \rightarrow d$ absorption spectra of $BaSO_4$:Ru^{6+} at 15 K (solid lines). Designation of the bands is given in C_{2v} notation with the T_d parent term added in brackets. In each graph the two Gaussians (dotted lines) were calculated with the fit parameters in Table 1; their sums are shown by the broken lines.

are listed in Table 1. Note that in **c** polarization the $^3T_2$ absorption is considerably weaker than in **a** and **b** polarizations.

The spectra in Figure 3 provide the key for an understanding of the strong dichroism observed in $BaSO_4$:Ru^{6+} crystals. In **a** polarization both red and green are absorbed by the $^3T_2/^3T_1$ transitions, resulting in the blue transmitted light. For **E**||**b** the $^3T_2/^3T_1$ absorptions are shifted to the red and the shoulder on the low-energy side of the LMCT 1 band cuts the blue edge (see Figure 2), causing the green color. The red color in **c** polarization is due to the strong $^3T_1$ absorption in the green/blue region and the low intensity of $^3T_2$ in the red.

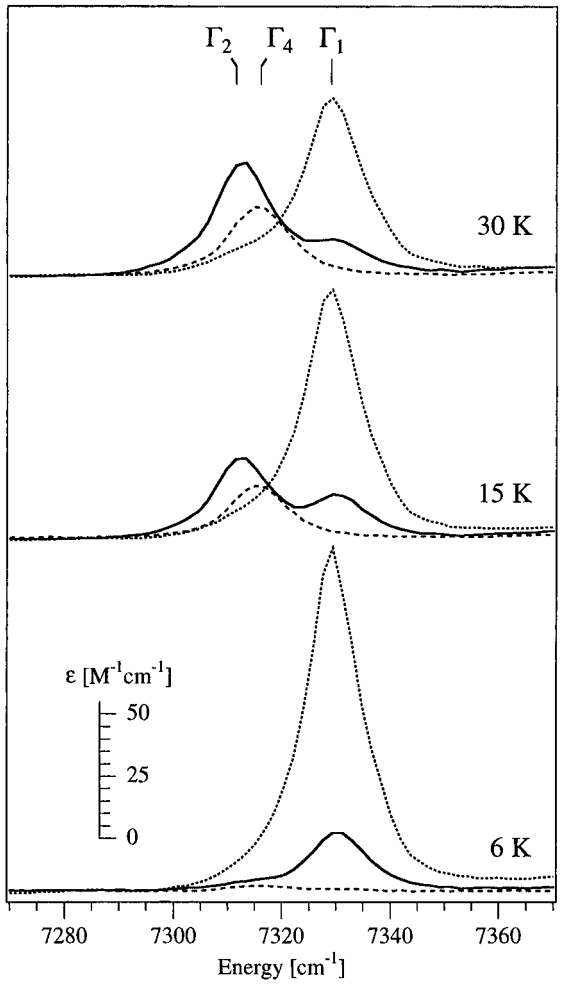

Figure 4. Temperature dependence of the $^1A_1$ absorption region of $BaSO_4$:Ru^{6+}. The **E**||**a**, **E**||**b**, and **E**||**c** polarized spectra are shown by solid, broken, and dotted lines, respectively. The ground-state spinor components are indicated in the C_{2v} double group.

Table 1. Band Maxima $\tilde{\nu}_{max}$, Molar Extinction Coefficients ϵ_{max}, Bandwidths at Half-Maximum $\tilde{\nu}_{1/2}$, and Oscillator Strengths f for the $^3A_2 \rightarrow {}^3T_2$, $^3T_1$ ($d \rightarrow d$) transitions of RuO_4^{2-} in $BaSO_4$, Obtained from Gaussian Resolutions of the Polarized Spectra in Figure 3

	E||**a**	**E**||**b**	**E**||**c**
	$^3A_2 \rightarrow {}^3T_2$		
C_{2v} label	$^3B_2$	$^3B_1$	$^3A_1$
$\tilde{\nu}_{max}$ (cm^{-1})	13 950	13 000	14 750
ϵ_{max} (M^{-1} cm^{-1})	100	132	52
$\tilde{\nu}_{1/2}$ (cm^{-1})	1950	1915	2150
$10^3 f$	0.9	1.2	0.5
	$^3A_2 \rightarrow {}^3T_1$		
C_{2v} label	$^3B_2$	$^3B_1$	$^3A_2$
$\tilde{\nu}_{max}$ (cm^{-1})	17 050	15 550	19 150
ϵ_{max} (M^{-1} cm^{-1})	384	243	345
$\tilde{\nu}_{1/2}$ (cm^{-1})	4150	4000	4250
$10^3 f$	7.4	4.5	6.7

In Figure 4 we show the temperature dependence of the $^1A_1$ absorption region in the near-IR of $BaSO_4$:Ru^{6+}. At 6 K a single sharp line peaks at 7329 cm^{-1} predominantly for **E**||**c**. With increasing temperature two hot bands at 7316 and 7311 cm^{-1} appear in the **b** and **a** polarizations, respectively. This is a clear indication for a 3-fold ground-state splitting of RuO_4^{2-} in the $BaSO_4$ host, and we can analyze the temperature dependence of the relative line intensities in terms of a Boltzmann population. In Figure 5 the intensity ratios of the two lines at 7316 and 7311 cm^{-1} to the one at 7329 cm^{-1} are shown by

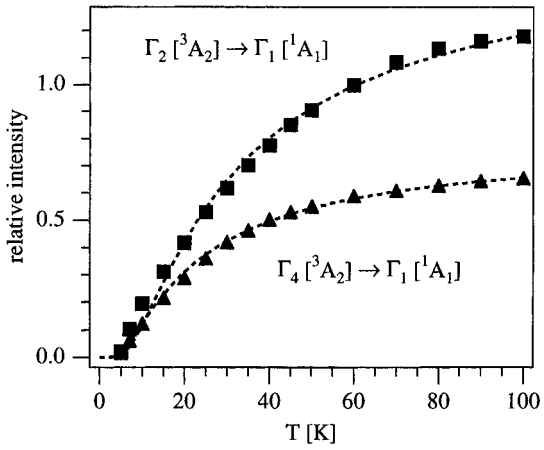

Figure 5. Temperature dependence of the line intensities of Γ_2 (squares) and Γ_4 (triangles) relative to Γ_1 for the $^1A_1$ absorption of RuO_4^{2-} in $BaSO_4$. See Figure 4 for band designations. The broken lines were obtained from a Boltzmann fit with three levels at 0, 13, and 18 cm^{-1}, respectively.

Table 2. Average Band Maxima (in cm^{-1}) for the $d \rightarrow d$ Transitions of RuO_4^{2-} in the Barite and β-K_2SO_4 Type Hosts Used for the Present Study[a]

transition	$BaSO_4$	$BaCrO_4$	$BaSeO_4$	K_2CrO_4	K_2SeO_4	Cs_2MoO_4
$^3A_2 \rightarrow {}^1A_1$	7 330	7 115	7 200	6 965	7 015	6 950
$^3A_2 \rightarrow {}^3T_2$	13 900	13 750	13 800	13 300	13 415	13 150
$^3A_2 \rightarrow {}^3T_1$	17 250	16 600	17 100	15 950	16 250	16 100

[a] Symmetry labels are given in the T_d point group.

triangles and squares, respectively. The broken lines were obtained from a Boltzmann fit with three levels at 0, 13, and 18 cm^{-1}, respectively. The correspondence with the experimental data is excellent. The intensity ratios of the hot to the cold components extrapolated for $T \rightarrow \infty$ are 0.79 and 1.53 for the lines at 7316 and 7311 cm^{-1}, respectively.

The absorption spectra of RuO_4^{2-} in the $BaCrO_4$ and $BaSeO_4$ hosts, which are not presented here, are similar to those of $BaSO_4$:Ru^{6+} shown in Figure 2. The band positions are listed in Table 2; band designations are according to Figure 2. For $BaCrO_4$:Ru^{6+} the upper limit of the measurable range is 20 000 cm^{-1}, given by the strong host absorption, and the overall ground-state splitting of RuO_4^{2-} is 19 cm^{-1}. In the $BaSeO_4$ host the $^1A_1$ absorption is much broader and the ground-state splitting thus unresolved.

Figure 6 shows the **E**||**b** polarized 15 K absorption spectrum of K_2SeO_4:Ru^{6+}. The spectrum is very similar in general appearance to those of $BaSO_4$:Ru^{6+} in Figure 2, consisting of a weak sharp feature in the near-IR (labeled $^1A_1$ in Figure 6), a broad band in the vis ($^3T_1$) with a shoulder on its low-energy side ($^3T_2$), and two intense LMCT bands above 22 000 cm^{-1} (LMCT 1 and 2, respectively). Six members of a progression in 760 cm^{-1} can be made out for the LMCT 1 band. The **E**⊥**b** spectrum of K_2SeO_4:Ru^{6+} and the spectra of RuO_4^{2-} doped into the isostructural K_2CrO_4 and Cs_2MoO_4 hosts look very similar to the one in Figure 6. The band positions in the three hosts are included in Table 2.

The $^1A_1$ absorption region of K_2SeO_4:Ru^{6+} is shown on an expanded scale in the inset of Figure 6. Similar to $BaSO_4$:Ru^{6+} (Figure 4), we observe three closely spaced lines at 7006, 7014, and 7023 cm^{-1}, respectively. Yet their relative intensities are temperature independent and thus inconsistent with a 3-fold ground-state splitting of RuO_4^{2-}. In this case the presence of three lines is due to crystallographic phase transitions occurring at 128 and 93 K.[19] In the *Pna*2$_1$ low-temperature phase of K_2SeO_4 there are three crystallographically inequivalent SeO_4^{2-}

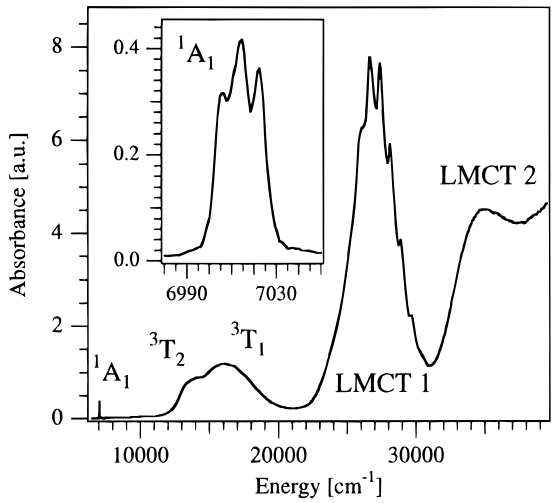

Figure 6. **E**||**b** polarized 15 K absorption spectrum of K_2SeO_4:Ru^{6+}. $d \rightarrow d$ band designations are given in T_d notation. Ligand-to-metal charge-transfer bands are labeled LMCT 1/2. The inset shows the $^1A_1$ absorption region on an expanded scale.

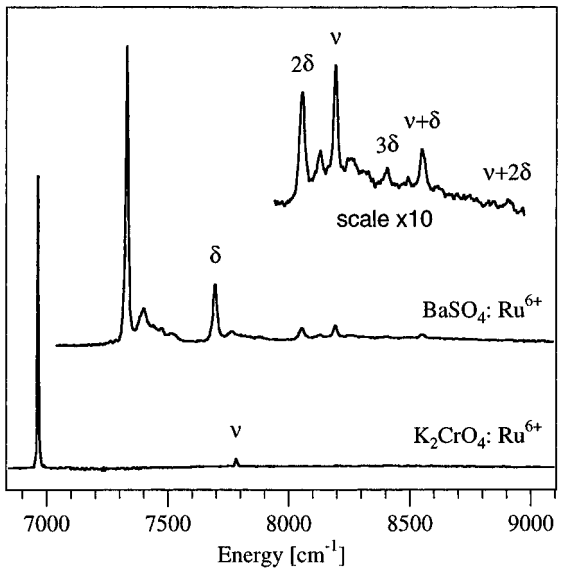

Figure 7. Comparison of the $^1A_1$ absorption regions of RuO_4^{2-} in K_2CrO_4 (unpolarized, 15 K) and $BaSO_4$ (**E**||**c**, 6 K). Vibrational sidebands for progressions in the O−Ru−O bending (δ) and Ru−O stretching (ν) modes are indicated.

sites,[20] giving rise to the tripling of the $^1A_1$ line in Figure 6. Similar effects were observed in the optical spectra of K_2SeO_4:Fe^{6+} [18] and K_2SeO_4:Mn^{6+}.[21] In the isostructural K_2CrO_4 and Cs_2MoO_4 hosts the $^1A_1$ absorption regions consist of a single line with a half-width of about 5 cm^{-1}, giving an upper limit for the ground-state splittings of RuO_4^{2-} of 5 cm^{-1}.

Figure 7 compares the $^1A_1$ absorption regions of RuO_4^{2-}-doped K_2CrO_4 and $BaSO_4$ at low temperatures. The sideband structures built on the electronic origins at 6965 and 7329 cm^{-1}, respectively, are strikingly different. In the spectrum of K_2CrO_4:Ru^{6+} we observe a single sideband of low intensity due to the totally symmetric Ru−O stretching (ν) mode of 817 cm^{-1}. The corresponding Huang-Rhys parameter which is defined by the intensity ratio of the first sideband to the respective origin line is $S_\nu = 0.04$. For $BaSO_4$:Ru^{6+} three members of a progression in the O−Ru−O bending (δ) mode of 365 cm^{-1}

(19) Chaudhuri, B. K.; Atake, T.; Chihara, H. *Solid State Commun.* **1981**, *38*, 927.
(20) Yamada, N.; Ono, Y.; Ikeda, T. *J. Phys. Soc. Jpn.* **1984**, *53*, 2565.
(21) Brunold, T. C.; Hazenkamp, M. F.; Güdel, H. U. *J. Am. Chem. Soc.* **1995**, *117*, 5598.

with $S_\delta = 0.26$ and a series of low-frequency phonon modes coupling to the electronic transition can be made out in addition to the progression in the ν mode of 863 cm^{-1} ($S_\nu = 0.04$).

The successful application of Cr(IV)-doped forsterite (Mg_2SiO_4:Cr^{4+}) as tunable solid-state laser material[22,23] has triggered a flurry of spectroscopic and laser oriented studies of $3d^2$ tetraoxo complexes.[18,24−33] It was found that the CrO_4^{4-}, MnO_4^{3-}, and FeO_4^{2-} ions all exhibit strong luminescence in the near-IR persisting up to room temperature. We therefore tried very hard to detect luminescence from our RuO_4^{2-}-doped crystals. However, down to 3500 cm^{-1} we were not able to observe luminescence from any of our RuO_4^{2-}-doped samples even at low temperatures.

4. Discussion

4.1. Band Assignments in the T_d Approximation. With the exception of K_2SeO_4 at low temperatures[20] the space group of the host lattices used for the present study is *Pnma*.[17] The only symmetry element of the host tetrahedra is a mirror plane perpendicular to the crystallographic **b** axis, and the site symmetry is thus reduced to C_s. In the low-temperature phase of K_2SeO_4 (space group $Pna2_1$[20]) the symmetry of the three crystallographically inequivalent SeO_4^{2-} ions is further reduced to C_1.[20]

However, the site symmetry in the various hosts is close to tetrahedral, particularly in those with the β-K_2SO_4 structure, and in a first approximation we analyze the absorption spectra presented in Figures 2−4 and 6 in the parent T_d point group. The effect of the C_s site perturbation is greatest in the barite-type hosts, and it will be considered in the following section.

From the Tanabe−Sugano diagram for a d^2 ion in T_d symmetry we expect three spin-allowed $d \rightarrow d$ absorptions of RuO_4^{2-}, i.e. $^3A_2 \rightarrow {}^3T_2$, $^3T_1$, and $^3T_1$*(t_2^2). In T_d only the two $^3T_1$ excitations are symmetry allowed, but $^3A_2 \rightarrow {}^3T_1$*($t_2^2$) involves a two-electron excitation and therefore carries low intensity. It is thus relatively straightforward to assign the broad band peaking around 16 500 cm^{-1} in the spectra of $BaSO_4$:Ru^{6+} (Figures 2 and 3) and K_2SeO_4:Ru^{6+} (Figure 6) to $^3A_2 \rightarrow {}^3T_1$ and the shoulder on its low-energy side at about 13 500 cm^{-1} to $^3A_2 \rightarrow {}^3T_2$. The $^3A_2 \rightarrow {}^3T_2$ splitting directly corresponds to the ligand-field strength $10Dq$, giving a value of $10Dq \approx 13\,500$ cm^{-1}.

Two weak sharp lines are expected for the spin-flip transitions $^3A_2 \rightarrow {}^1E$ and $^1A_1$, respectively. ^1E splits upon symmetry lowering to C_s, and we expect a pair of two closely spaced lines rather than a single line in the hosts used for the present study. This has been observed for the ^1E absorption of the $3d^2$ ions MnO_4^{3-} [31] and FeO_4^{2-} [18] in C_s symmetry. Therefore we assign the sharp line peaking around 7000 cm^{-1} in Figures 2 and 6 to the $^3A_2 \rightarrow {}^1A_1$ spin-flip transition.

This assignment suggests the ^1E absorption to occur at about 3800 cm^{-1}. This is a very difficult spectral region because of the intense absorptions due to H_2O vibrations. Despite numerous attempts we were not able to identify the $^3A_2 \rightarrow {}^1E$ absorption in any of our crystals. We did observe an **a** polarized very weak line at 3633 cm^{-1} which was absent in undoped $BaSO_4$. However, from its temperature dependence we can exclude that it is due to RuO_4^{2-}. This is supported by the lower intensity of this line relative to the $d \rightarrow d$ bands in a $BaSO_4$:Ru^{6+} sample prepared under different conditions (section 2.1). A more likely explanation of this line is an O−H stretch vibration of traces of *trans*-$Ru(OH)_2O_3^{2-}$ doped into $BaSO_4$.

The fact that $^1A_1$ lies far below $^3T_2$ indicates that we must be to the extreme right in the Tanabe−Sugano diagram. Indeed, by fitting the three experimental transition energies in a ligand-field calculation we obtain values for $10Dq/B_{complex}$ of about 55 in every host, where $B_{complex} \approx 245$ cm^{-1} is the Racah parameter of Ru in the complex and a ratio of $C/B = 3.7$ was assumed. An explanation for this unusually large $10Dq/B_{complex}$ value will be given in section 4.4.

The highest-energy completely occupied set of molecular orbitals transforms as t_1 and is purely ligand centered. Hence promotion of an electron from t_1 to e formally corresponds to a ligand-to-metal charge-transfer (LMCT) excitation. The resulting electron configuration is $t_1^5e^3$ with the corresponding triplet LMCT states $^3T_1$ and $^3T_2$. Only $^3T_1$ excitations are symmetry allowed, and it is thus straightforward to assign the strong LMCT 1 band in Figures 2 and 6 to $^3A_2 \rightarrow {}^3T_1$ ($t_1 \rightarrow e$). The $^3A_2 \rightarrow {}^3T_2$ ($t_1 \rightarrow e$) transition is assumed to borrow intensity from the nearby LMCT 1 transition through spin−orbit coupling and the low-symmetry crystal field, and we assign the shoulder at 23 500 cm^{-1} in the $\mathbf{E}||\mathbf{b}$ spectrum of $BaSO_4$:Ru^{6+} (Figure 2) to that transition. Although there is no such feature in the spectrum of K_2SeO_4:Ru^{6+}, both the unresolved vibrational structure in the origin region and the asymmetric shape of the LMCT 1 band indicate the overlap with a weak band on its low-energy side.

From the vibrational structure observed on the LMCT 1 band in the spectrum of K_2SeO_4:Ru^{6+} (see Figure 6) we find a frequency of 760 cm^{-1} for the totally symmetric stretch vibration in the $^3T_1$ ($t_1 \rightarrow e$) state. The corresponding frequency in the $^1A_1$ state is 820 cm^{-1}, and we would expect a similar value in the ground state. This indicates that the Ru−O bonds become substantially weaker upon LMCT excitation.

It is clear that the main reason for the poor agreement between calculated and observed spectra of ruthenate(VI) in the past is the erroneously assumed tetraoxo coordination of ruthenium(VI). It is thus interesting to use the spectra presented here for a comparison with calculated transition energies of RuO_4^{2-}. On the basis of a Hartree−Fock−Slater discrete variational method calculation, which appears to be the most sophisticated calculation for RuO_4^{2-} so far, it was suggested a long time ago that the $^3T_1$ ($d \rightarrow d$) and first two $^3T_1$ LMCT absorptions should be observed at 12 000, 25 000, and 36 000 cm^{-1}, respectively.[11] These numbers are in reasonable agreement with our experimental values of about 16 500, 26 000, and 32 000 cm^{-1}, respectively. In contrast, they are in very poor agreement with the band positions in the ruthenate(VI) spectrum (see Figure 1). The discrepancy has so far been blamed on the calculation. We now realize that the experimental result was not correct and the calculation pretty good.

4.2. Low-Symmetry Splittings in the Absorption Spectrum of $BaSO_4$:Ru^{6+}. In $BaSO_4$ the O−S−O angles of the

(22) Petricevic, V; Gayen, S. K.; Alfano, R. R. *Appl. Phys. Lett.* **1988**, *53*, 2590.
(23) Verdun, H. R.; Thomas, L. M.; Andrauskas, D. M.; McCollum, T.; Pinto, A. *Appl. Phys. Lett.* **1988**, *53*, 2593.
(24) Eilers, H.; Hömmerich, U.; Jacobsen, S. M.; Yen, W. M.; Hoffman, K. R.; Jia, W. *Phys. Rev.* **1994**, *B49*, 15505.
(25) Kück, S.; Petermann, K.; Pohlmann, U.; Schönhoff, U.; Huber, G. *Appl. Phys.* **1994**, *B58*, 153.
(26) Reinen, D.; Kesper, U.; Atanasov, M.; Roos, J. *Inorg. Chem.* **1995**, *34*, 184.
(27) Hazenkamp, M. F.; Güdel, H. U.; Atanasov, M.; Kesper, U.; Reinen, D. *Phys. Rev.* **1996**, *B53*, 2367.
(28) Lachwa, H.; Reinen, D. *Inorg. Chem.* **1989**, *28*, 1044.
(29) Capobianco, J. A.; Cormier, G.; Moncorgé, R.; Manaa, H. *J. Lumin.* **1992**, *54*, 1.
(30) Merkle, L. D.; Pinto, A.; Verdun, H. R.; McIntosh, B. *Appl. Phys. Lett.* **1992**, *61*, 2368.
(31) Oetliker, U.; Herren, M.; Güdel, H. U.; Kesper, U.; Albrecht, C.; Reinen, D. *J. Chem. Phys.* **1994**, *100*, 8656.
(32) Merkle, L. D.; Guyot, Y.; Chai, B. H. T. *J. Appl. Phys.* **1995**, *77*, 474.
(33) Brunold, T. C.; Güdel, H. U.; Kück, S.; Huber, G. *J. Lumin.* **1996**, *65*, 293.

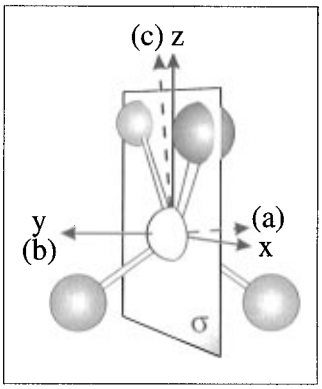

Figure 8. Schematic illustration of the RuO_4^{2-} ion in the $BaSO_4$ host. The crystallographic and molecular axes are denoted by **a**, **b**, **c** and **x**, **y**, **z**, respectively. The only symmetry element is a mirror plane σ perpendicular to **y**(**b**), but the symmetry is approximately C_{2v}, the **z** axis being the pseudo C_2 axis.

sulfate ion vary between 105.9 and 114.1°,[17] and the deviations from T_d symmetry are thus substantial. The SO_4^{2-} site symmetry is C_s, but the symmetry lowering corresponds, in essence, to a $T_d \rightarrow C_{2v}$ distortion. Therefore we analyze the spectra of $BaSO_4$:Ru^{6+} in the C_{2v} approximation. This approach is based on the successful interpretation of the MnO_4^{3-} and MnO_4^{2-} spectra in $BaSO_4$ assuming an approximate C_{2v} symmetry.[35,36] The convention used for the orientation of the molecular **x**, **y**, **z** axes of $S(Ru)O_4^{2-}$ is illustrated in Figure 8. The pseudo C_2 (**z**) axis bisects the angle between the two oxygens above and below the C_s mirror plane σ. Both the **x** and **z** axes lie in the mirror plane σ, rotated by 8° from the **a** and **c** axes, respectively. **y** is perpendicular to σ and coincides with the **b** axis. The **a**, **b**, and **c** polarized crystal spectra in Figures 2−4 thus correspond in a good approximation to the **x**, **y**, and **z** polarized molecular spectra.

The splitting of the relevant ligand-field states of RuO_4^{2-} upon $T_d \rightarrow C_{2v}$ distortion is illustrated in Figure 9. Electric-dipole allowed transitions from the $^3A_2$ ground state are shown by arrows: solid, broken, and dotted lines correspond to **x**(**a**), **y**(**b**), and **z**(**c**) polarized transitions, respectively. With this polarization information we can readily identify the orbital components of the $^3T_2$ and $^3T_1$ states; the assignment is given in Figure 3 and the relevant numbers characterizing the transitions are collected in Table 1. In C_{2v} symmetry the $^3A_2 \rightarrow {}^3T_2$ transition is forbidden in **z** polarization and therefore appears only as a weak shoulder in the **E**||**c** spectrum (see Figure 3). However, its presence indicates that the selection rule is slightly relaxed. This is likely due to the combined action of the additional $C_{2v} \rightarrow C_s$ distortion and spin−orbit coupling.

By inspection of Figure 3 and Table 1 we note that the bandwidths for the $^3T_1/^3T_2$ absorptions differ by a factor of about 2. This can be qualitatively understood in terms of a simple model[37] assuming the bandwidths to be governed by the slopes of their transition energies with respect to variations in all ligand-field parameters with changing geometry. Table 1 shows that the ratio of the total $^3T_1/^3T_2$ splittings and thus the ratio of the geometry dependence of the $^3T_1/^3T_2$ transition energies (i.e. their slopes) is close to 2. Therefore we expect the corresponding bandwidths to differ by a factor of about 2, in good agreement with the experimental finding.

Let us now consider the effect of spin−orbit (SO) coupling in the approximate C_{2v} symmetry for the $^3A_2 \rightarrow {}^1A_1$ transition.

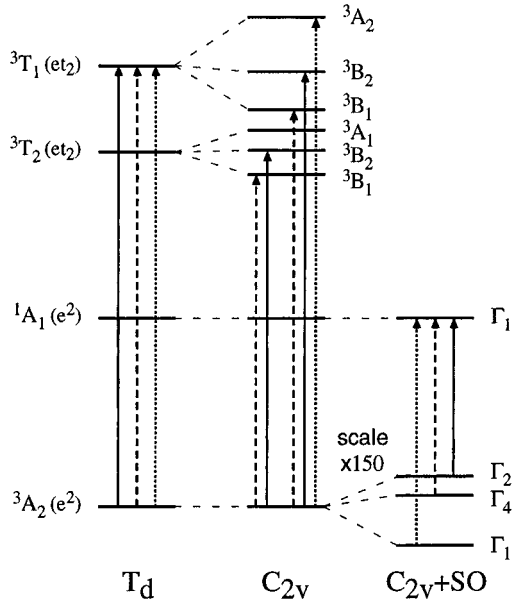

Figure 9. $T_d \rightarrow C_{2v}$ splitting of the relevant ligand-field states of RuO_4^{2-}. In T_d symmetry electron configurations are given in parentheses. Splittings relate to the polarized spectra in Figures 4 and 5 and are drawn to scale. Electric-dipole allowed transitions from the ground state are indicated by arrows: Solid, broken, and dotted lines are **x**(**a**), **y**(**b**), and **z**(**c**) polarized, respectively. The effect of spin−orbit (SO) coupling is sketched for the $^3A_2 \rightarrow {}^1A_1$ transition on the right-hand side (note the scale change).

As sketched on the right-hand side of Figure 9 the $^3A_2$ ground state splits into the three spinor components Γ_1, Γ_4, Γ_2, and we expect three differently polarized transitions to $\Gamma_1[^1A_1]$. Accordingly, the observed clear-cut polarization of the three lines in Figure 4 allows an unambiguous identification of the three components; the result is shown in Figure 9.

In T_d symmetry the $^1A_1$ state cannot mix with the adjacent $^3T_2$ state through spin−orbit coupling in first order, and it is therefore assumed to borrow its intensity from $^3A_2 \rightarrow {}^3T_1$. This is supported by the roughly constant value for the intensity ratios of the $^1A_1/^3T_1$ absorptions in the three polarizations, in contrast to the corresponding $^1A_1/^3T_2$ intensity ratios.

An interesting effect is observed in the $^1A_1$ absorption region of RuO_4^{2-} when we look at different host lattices. As shown in Figure 7 the vibrational sideband intensity is very different in the host lattices $BaSO_4$ and K_2CrO_4. Both the $^3A_2$ ground and $^1A_1$ excited states are orbitally nondegenerate and only the totally symmetric breathing (ν) mode can thus couple to the $^3A_2 \rightarrow {}^1A_1$ transition in T_d symmetry. However, on lowering the symmetry to C_s both the e and t_2 bending (δ) modes acquire some totally symmetric character and may thus also couple to this transition. Hence the Huang−Rhys parameter S_δ can be used as a measure for the distortion of the RuO_4^{2-} ion in a certain host lattice. The experimental S_δ values are ≈0 and 0.26 for K_2CrO_4:Ru^{6+} and $BaSO_4$:Ru^{6+}, respectively (see Figure 7). The strikingly different sideband intensity for the δ progression in these hosts is thus readily explained in terms of the different site distortions which is much stronger in $BaSO_4$. The mean deviations of the O−M−O angles φ_i from the tetrahedral angle $\varphi_{T_d} = 109.5°$, given by $\Delta\varphi = {}^1/_6\sum_{i=1}^{6}|\varphi_i - \varphi_{T_d}|$, are 0.5 and 2.2° in K_2CrO_4 and $BaSO_4$, respectively.[17] In contrast, the Huang−Rhys parameter S_ν is very similar in all the hosts and only about 0.04. This low value reflects the minor change in the Ru−O bond length upon $^1A_1$ excitation, as we expect for a spin-flip transition.

Recently, the RuO_4^{2-} ion has been the subject of a theoretical study using density functional theory.[38] While the computed

(34) Moore, C. E. *Atomic Energy Levels*; NSRDS-NBS 35, U.S. Governmental Printing Office: Washington, DC, 1971.
(35) Brunold, T. C.; Güdel, H. U. *Chem. Phys. Lett.* **1996**, *257*, 123.
(36) Brunold, T. C.; Güdel, H. U. *Inorg. Chem.*, in press.
(37) Gerloch, M. *Comments Inorg. Chem.* **1996**, *18*, 101.

Ru−O distances of RuO_4 and RuO_4^- were found in good agreement with experiment, the bond length in RuO_4^{2-} was calculated significantly too long. It was then suggested that the accepted picture of the electronic structure of RuO_4^{2-} may need a revision. The ground state of RuO_4^{2-} was postulated to be ^3E with an $e^1a_1^1$ electron configuration rather than $^3A_2$ (e^2), where a_1 is a mainly Ru centered molecular orbital with a strong 5s character. However, the spectroscopic results presented here clearly demonstrate that ligand-field theory is valid, the ground state thus a $^3A_2$ as in the corresponding $3d^2$ complexes CrO_4^{4-}, MnO_4^{3-}, and FeO_4^{2-}. The involvement of the a_1 molecular orbital in the results of ref 38 must be an artifact of the calculation. We suspect that it might be due to an insufficient definition of the 5s basis functions.

4.3. Assignment of the Ruthenate(VI) Spectrum, *trans*-$Ru(OH)_2O_3^{2-}$. The assignment of the absorption spectrum of *trans*-$Ru(OH)_2O_3^{2-}$ has been the subject of much confusion in the past. First we note that in the spectra of RuO_4, $4d^0$, and RuO_4^-, $4d^1$ (not shown), the first observable absorptions peak at 26 000 and 32 000 cm^{-1}, respectively,[2] matching closely in position and oscillator strength the LMCT 1 and 2 bands of RuO_4^{2-} in Figure 1. This demonstrates that the effective charge on ruthenium in these three complexes is roughly the same although its formal charge increases from +6 to +8 along the series RuO_4^{2-}, RuO_4^-, and RuO_4. This is supported by the similar values reported for the average Ru−O bond lengths of 1.76 Å in Cs_2RuO_4,[16] 1.79 Å in $KRuO_4$,[39] and 1.71 Å in RuO_4.[40]

In comparison with $BaSO_4$:Ru^{6+}, the first two strong absorptions in the ruthenate(VI) spectrum, peaking at 21 500 and 27 000 cm^{-1}, respectively, are red-shifted by about 6000 cm^{-1}; see Figure 1. However, they are very similar in shape and intensity to the LMCT 1 and LMCT 2 bands of RuO_4^{2-}, respectively. We therefore assign them to charge-transfer rather than $d \rightarrow d$ transitions. From a chemical viewpoint it seems reasonable[41] that, provided the electron affinity is higher for hydroxide than oxide as we would expect, these bands can be assigned to O → Ru charge-transfer bands.

This assignment is supported by the following considerations. From the crystal structures of Cs_2RuO_4[16] and $K_2Ru(OH)_2O_3$[14,15] it is known that the equatorial ruthenium−oxygen bond lengths in the latter are the same as in RuO_4^{2-}. Therefore, on going from RuO_4^{2-} to *trans*-$Ru(OH)_2O_3^{2-}$, we just need to consider the effect of replacing one oxygen by two hydroxides and a spatial rearrangement of the other three oxygens. We expect an increase in both the ligand-field strength at the Ru site and the effective positive charge on ruthenium. This explains the observed red-shift of the O → Ru LMCT absorptions (see Figure 1) and suggests a blue-shift for the $d \rightarrow d$ transitions. With the $d \rightarrow d$ bands of RuO_4^{2-} occurring in close energetic vicinity to the first LMCT band of *trans*-$Ru(OH)_2O_3^{2-}$, see Figure 1, the $d \rightarrow d$ absorptions of ruthenate(VI) are likely superimposed by the stronger LMCT bands.

We performed an extended Hückel molecular-orbital calculation[42] for the three complexes $Ru(OH)_4^{2+}$ (hypothetical), RuO_4^{2-}, and *trans*-$Ru(OH)_2O_3^{2-}$ to verify our assignment of the ruthenate(VI) spectrum based on qualitative arguments. For the calculations we assumed T_d symmetry for $Ru(OH)_4^{2+}$, RuO_4^{2-}, and D_{3h} symmetry for *trans*-$Ru(OH)_2O_3^{2-}$. The Ru−O and Ru−OH bond lengths of 1.76 and 2.03 Å, respectively, were taken from the $K_2Ru(OH)_2O_3$ crystal structure,[14,15] and the hydrogens were placed along the Ru−OH bonds at a distance of 0.85 Å from the corresponding oxygens. In Figure 10 the relevant molecular orbitals are plotted relative to the set of half-filled e molecular orbitals. In $Ru(OH)_4^{2+}$ the fully occupied mainly ligand-centered orbitals are substantially lower in energy than in the RuO_4^{2-} and *trans*-$Ru(OH)_2O_3^{2-}$ complexes (shaded areas in Figure 10). This supports our assignment of the first observable bands in the ruthenate(VI) spectrum (Figure 1) to O → Ru rather than HO → Ru CT transitions. The calculation predicts that the lowest-energy LMCT bands are slightly red-shifted in the spectrum of *trans*-$Ru(OH)_2O_3^{2-}$ relative to RuO_4^{2-}, as observed (Figure 1). It also suggests a marked increase in ligand-field strength on going from RuO_4^{2-} to *trans*-$Ru(OH)_2O_3^{2-}$, thus confirming our assumption that the $d \rightarrow d$ bands in the spectrum of ruthenate(VI) are hidden by the intense LMCT absorptions.

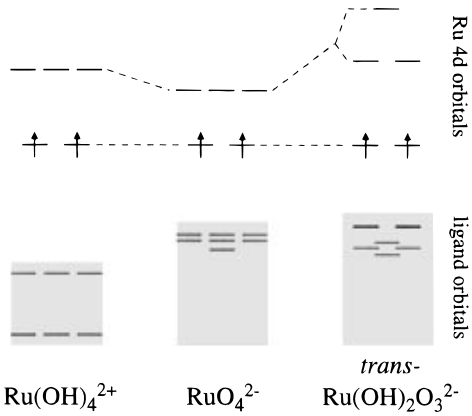

Figure 10. Plot of the relevant molecular orbitals of $Ru(OH)_4^{2+}$, RuO_4^{2-}, and *trans*-$Ru(OH)_2O_3^{2-}$ relative to the respective set of e molecular orbitals, obtained from an extended Hückel molecular-orbital calculation. The shaded areas mark the fully occupied mainly ligand-centered orbitals.

Table 3. Comparison of Spectroscopic Data for the $3d^2$ Ions CrO_4^{4-}, MnO_4^{3-}, and FeO_4^{2-} and the $4d^2$ Ion RuO_4^{2-}

	CrO_4^{4-} [a]	MnO_4^{3-} [b]	FeO_4^{2-} [c]	RuO_4^{2-}
host	Ca_2GeO_4	Ca_2VO_4Cl	K_2SO_4	$BaSO_4$
$\Delta\varphi$ (deg)[d]	6.5	4.5	0.3[e]	2.2[e]
r_{M-O} (Å)	1.76	1.70	1.65	1.76
$10Dq$ (cm^{-1})	9000	10 500	13 000	13 900
$B_{complex}$ (cm^{-1})[f]	540	500	370	255
$\beta = B_{complex}/B_0$[g]	0.54	0.42	0.27	0.28
$10Dq/B_{complex}$	17	21	35	55
$\tilde{\nu}_{max}$(LMCT 1) (cm^{-1})	43 000	33 000[h]	21 000	27 700
f(LMCT 1)	0.1	0.1[h]	0.02	0.03
$10^3 f(^3A_2 \rightarrow {}^3T_2)$	0.05	1.0	8	0.9
$10^3 f(^3A_2 \rightarrow {}^3T_1)$	1	9	≈16	6.2
$\zeta_{complex} = \beta\zeta_0$ (cm^{-1})[i]	170	200	180	550
$^3A_2$ splitting (cm^{-1})	0.1	0.5	0.1	18

[a] From refs 26 and 27. [b] From refs 28 and 31. [c] From refs 33 and 43. [d] Average deviation from tetrahedral angle $\varphi_{T_d} = 109.5°$ for the host tetrahedron: $\Delta\varphi = {}^1/_6\sum_{i=1}^{6}|\varphi_i - \varphi_{T_d}|$. [e] From ref 17. [f] From fits of the experimental transition energies in the framework of a ligand-field calculation using the free-ion ratios C_0/B_0 of 4.2 (CrO_4^{4-}),[27] 4.35 (MnO_4^{3-}),[31] 3.70 (FeO_4^{2-}),[33] and 3.70 (RuO_4^{2-}, according to FeO_4^{2-}). [g] Free-ion values B_0 from ref 34, extrapolated for Ru^{6+}. [h] In aqueous solution, from ref 44. [i] Free-ion values ζ_0 from ref 45, extrapolated for Ru^{6+}.

4.4. Comparison of Spectroscopic Data of RuO_4^{2-} with CrO_4^{4-}, MnO_4^{3-}, and FeO_4^{2-}. Table 3 offers a comparison of experimental spectroscopic data for the series of $3d^2$ ions

(38) Deeth, R. J. *J. Chem. Soc., Dalton Trans.* **1995**, 1537.
(39) Silverman, M. D.; Levy, H. A. *J. Am. Chem. Soc.* **1954**, *76*, 3317.
(40) Schaefer, L.; Seip, H. M. *Acta Chem. Scand.* **1967**, *21*, 737.
(41) Kläning, U.; Symons, M. C. R. *J. Chem. Soc.* **1961**, 3204.
(42) Calzaferri Group, ICONC computer program, release 1989; Departement für Chemie und Biochemie, Universität Bern, Freiestrasse 3, CH-3000 Bern 9, Switzerland.
(43) Wagner, B.; Reinen, D.; Brunold, T. C.; Güdel, H. U. *Inorg. Chem.* **1995**, *34*, 1934.
(44) Carrington, A.; Symons, M. C. R. *J. Chem. Soc.* **1956**, 3373.
(45) Bendix, J.; Brorson, M.; Schäffer, C. E. *Inorg. Chem.* **1993**, *32*, 2838.

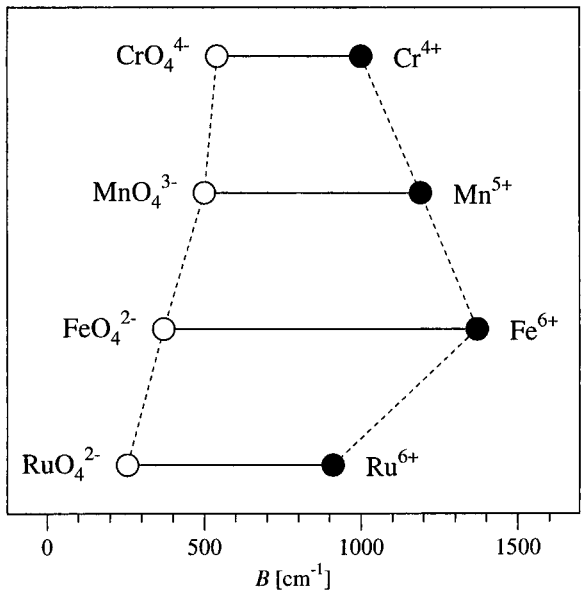

Figure 11. (●) Free-ion Racah parameters B_0 of four d^2 ions, from ref 34 and extrapolated for Ru^{6+}. (○) $B_{complex}$ values derived from fits of the experimental transition energies in terms of a ligand-field calculation. Data for the $3d^2$ complexes are taken from refs 27, 31, and 33.

CrO_4^{4-}, MnO_4^{3-}, and FeO_4^{2-} and the $4d^2$ ion RuO_4^{2-}, all in tetrahedral coordination. Although the distortions of the respective host tetrahedron (expressed in terms of $\Delta\varphi$) vary considerably, most of the parameters in Table 3 were found to be rather insensitive to the host, thus allowing a discussion of gross trends along this series.

With increasing formal charge on the metal ion the bond length r_{M-O} decreases and the ligand-field strength $10Dq$ increases along the series of $3d^2$ ions. Ligand-field theory predicts $10Dq$ to depend on the -5th power of r_{M-O}. The observed dependence is weaker. This is a consequence of increasing covalency along the series CrO_4^{4-}, MnO_4^{3-}, and FeO_4^{2-} which is nicely reflected by the decreasing value of the nephelauxetic ratio $\beta = B_{complex}/B_0$; see Table 3. FeO_4^{2-} and RuO_4^{2-} have similar β values of 0.27 and 0.28, respectively. In Figure 11 the $B_{complex}$ values obtained from fits of the experimental transition energies in a ligand-field calculation are plotted for the four complexes and compared to the corresponding B_0 values of the free ion. From CrO_4^{4-} to FeO_4^{2-} the increase in the covalency is so strong that the increase in the free-ion Racah parameter B_0 is more than compensated. B_0 is smaller for Ru^{6+} than for Fe^{6+}, and the $B_{complex}$ value is thus further reduced down the row FeO_4^{2-} to RuO_4^{2-}. In contrast, the $10Dq$ parameter follows an opposite trend; i.e., it increases along the series CrO_4^{4-}, MnO_4^{3-}, FeO_4^{2-} and down the row to RuO_4^{2-}, and we obtain the unusually large $10Dq/B_{complex}$ value of 55 for RuO_4^{2-}.

In first order the ground-state (GS) splitting is induced by spin−orbit (SO) interaction of the otherwise degenerate spinor components of $^3A_2$ with corresponding components of the $^3T_2$ state, which is split by the low-symmetry crystal field.[28] The GS splitting is then roughly given by $\zeta^2_{complex}\ \delta E/(10Dq)^2$,[46] where $\zeta_{complex}$ is the effective SO coupling parameter and δE the $^3T_2$ splitting. δE is expected to scale with the distortion $\Delta\varphi$. This is nicely confirmed by the small GS splitting of less than 5 cm^{-1} in K_2CrO_4 (see Figure 7) in which the Cr(VI) site symmetry is close to T_d with $\Delta\varphi = 0.5°$ [17] and the large splitting of 18 cm^{-1} at the strongly distorted sulfate site in $BaSO_4$ (Figure 4) with $\Delta\varphi = 2.2°$.[17] On the other hand, the GS splitting increases despite the decreasing value for $\Delta\varphi$ along the series CrO_4^{4-}, MnO_4^{3-}, and RuO_4^{2-}. This is qualitatively understood by the increasing value of the SO coupling parameter $\zeta_{complex}$, where we assume that $\zeta_{complex} = \beta\zeta_0$ (see Table 3).

The spin-allowed $d \rightarrow d$ transitions are assumed to borrow their intensity, in essence, from nearby LMCT transitions through the crystal field. As the charge on the metal ion increases, the first LMCT transition shifts to the red and the $^3T_2$, $^3T_1$ ($d \rightarrow d$) absorptions are thus expected to become stronger, in agreement with the experimental finding (see Table 3). Yet, in the case of MnO_4^{3-} and RuO_4^{2-}, this simple rule seems to be violated. However, in that case the larger separation between the $d \rightarrow d$ and LMCT transitions for MnO_4^{3-} is more than compensated by the higher intensity of the LMCT 1 absorption (see Table 3).

The intensities of the LMCT 1 absorptions of FeO_4^{2-} and RuO_4^{2-} are surprisingly low for charge-transfer transitions; see Table 3. Quantum theory predicts that for a constant transition dipole moment μ_{LMCT} the oscillator strength f scales linearly with the transition energy $\tilde{\nu}$; i.e. $f \propto \tilde{\nu}|\mu_{LMCT}|^2$.[47] The observed dependence is stronger, see Table 3, indicating that the transition dipole moment decreases as the formal charge of the metal ion increases. The same holds for the series of $3d^0$ ions VO_4^{3-}, CrO_4^{2-}, and MnO_4^{-}.[33] Along this series the oscillator strength f of the first allowed LMCT transition decreases from 0.15 to 0.09 and 0.03, while the peak position $\tilde{\nu}_{max}$ shifts from 36 900 to 26 800 and 18 300 cm^{-1}.[48] We ascribe this to the increasing covalency which lowers the transition dipole moment of charge-transfer transitions.

5. Conclusions

Despite the fact that the absorption spectrum of basic aqueous solutions of ruthenium(VI), i.e. the so-called ruthenate(VI) ion, has been widely used for the spectrophotometric determination of ruthenium, it has never been really understood because it has been ascribed to the wrong species. With the first absorption spectra of RuO_4^{2-} reported here we clear up the situation. The problem turns out to be an experimental rather than a computational one. The absorption spectrum of ruthenate(VI) solutions, erroneously assumed to contain RuO_4^{2-} for many years, is shown to be strikingly different from the real RuO_4^{2-} spectrum. The $4d^2$ ion Ru^{6+} is larger than the $3d^2$ ions Cr^{4+}, Mn^{5+}, and Fe^{6+}, and the preferred configuration in basic aqueous solutions is thus *trans*-$Ru(OH)_2O_3^{2-}$ rather than RuO_4^{2-}.

Under suitable conditions the RuO_4^{2-} ion can be stabilized in various crystal lattices, and its optical absorption spectrum can be studied in detail. The spectroscopic data for RuO_4^{2-} fit nicely into the trends observed for the series of $3d^2$ tetraoxo complexes, far exceeding their limits in many cases due to the different radial parts of 3d and 4d wave functions. Although with a value of 55 the relative ligand-field strength $10Dq/B_{complex}$ approaches the strong-field limit, ligand-field theory is still applicable.

Acknowledgment. This work was financially supported by the Swiss National Science Foundation.

IC961314J

(46) Abragam, A.; Bleaney, B. *Electron Paramagnetic Resonance of Transition Ions;* Clarendon Press: Oxford, U.K., 1970; pp 432, 440, 450.

(47) McGlynn, S. P.; Vanquickenborne, L. G.; Kinoshita, M.; Carroll, D. G. *Introduction to Applied Quantum Chemistry*; Holt, Rinehart and Winston: New York, 1972; p 299.

(48) Carrington, A.; Symons, M. C. R. *Chem. Rev.* **1963**, *63*, 443.